Journal of Aerosol Science 41 (2010) 1143–1151

Contents lists available at ScienceDirect

Journal of Aerosol Science

journal homepage: www.elsevier.com/locate/jaerosci

Characterization of a method for aerosol generation from heavy fuel oil (HFO) as an alternative to emissions from ship diesel engines

Zhongqing Zheng [a,b], Xiaochen Tang [b,c], Akua Asa-Awuku [b,c], Heejung S. Jung [a,b,*]

[a] Department of Mechanical Engineering, University of California, Riverside, CA 92521, USA
[b] Bourns College of Engineering, Center for Environmental Research and Technology (CE-CERT), 1084 Columbia Ave, Riverside, CA 92507, USA
[c] Department of Chemical and Environmental Engineering, University of California, Riverside, CA 92521, USA

ARTICLE INFO

Article history:
Received 10 June 2010
Received in revised form
28 September 2010
Accepted 4 October 2010
Available online 10 October 2010

Keywords:
Transition metal
Ash
Health effects
Nanoparticles
Ship emissions
Cloud condensation nuclei

ABSTRACT

This work describes a laboratory method to synthesize aerosols with properties similar to those emitted by ocean going ships. In this method, an oxy-hydrogen flame burner nebulizes and combusts heavy fuel oil (HFO). The oil was fed to the burner via a syringe pump at a maximum rate of 15 ml/h. Adjusting the feed temperature of the oil and the use of a quenching ring in the burner, it is possible to obtain an aerosol with a mode diameter of about 11 nm. This is close to the reported 5–8 nm for the nano-mode of ship emissions. Filter samples were also analyzed for elemental carbon, organic carbon and anion composition. No elemental carbon mass was detected and only a few sulfur containing compounds were present. A chemical equilibrium model was applied for both oxy-hydrogen flame and 2-stroke ship diesel engine combustion conditions to predict equilibrium concentrations, chemical formula and phase of vanadium and nickel containing compounds. The model confirmed that the real-world ship diesel engine and the oxy-hydrogen flame burner combustion processes produced the same vanadium, nickel and sulfur particulate matter (PM) products in terms of chemical formula and phase. Both the 5–8 nm particles from real-world ship emissions and the laboratory synthesized particles contain transition metals. Transmission electron microscope (TEM) images of laboratory synthesized particles show similar morphology to those sampled from a ship. Cloud condensation nuclei (CCN) measurement indicates that neither laboratory generated nor ship emitted aerosol is hygroscopic. To our knowledge, this is the first time the 5–8 nm particles emitted from ships have been aptly synthesized on a laboratory scale.

© 2010 Elsevier Ltd. All rights reserved.

1. Introduction

Freshly emitted particulate matter (PM) is ideal for *in vivo* and *in vitro* health effect studies. While researchers have relatively easy access to on-road engine and chassis dynamometer PM, it is difficult to directly explore the health impacts of PM from ships. Few manufacturers (Man B&W, Wartsila and Mitsubishi) control more than 80% of ship engine market share and even they have very few engine dynamometers and scientists are rarely granted access to such extraordinary facilities (Kasper, Aufdenblatten, Forss, Mohr, & Burtscher, 2007). When direct engine PM emissions are not available, health scientists may use bulk PM samples. The National Institute of Standards and Technology (NIST) collects different

* Corresponding author. Tel.: +1 951 781 5742; fax: +1 951 781 5790.
E-mail address: heejung@engr.ucr.edu (H.S. Jung).

0021-8502/$ - see front matter © 2010 Elsevier Ltd. All rights reserved.
doi:10.1016/j.jaerosci.2010.10.002

and large amounts of diesel PM. The samples are commercially available standard reference materials (SRM). Diesel engine PM SRM has been resuspended into aerosol and extracted for *in vivo* and *in vitro* studies (Lippmann & Chen, 2009). But resuspended particles may not replicate freshly emitted particle size and number distribution. Furthermore (as of September 2010), there is no available NIST ship engine PM SRM. Only recently have PM ship studies gained either on-board or aircraft measurement access (Agrawal et al., 2008; Murphy et al., 2009). Health related studies will benefit from an alternative method to access ship source PM.

Useful health information can be obtained from laboratory-generated particles (Brown, Wilson, MacNee, Stone, & Donaldson, 2001; Dick, Brown, Donaldson, & Stone, 2003; Gwinn & Vallyathan, 2006; Oberdorster, 2000; Oberdorster, Oberdorster, & Oberdorster, 2005; Pinkerton, 2002). Particle concentration, size, hygroscopicity, morphology, transition metal, organic and elemental carbon and composition adversely affect health (Albritton & Greenbaum, 1998; Blanchard & Willeke, 1984; Broday & Georgopoulos, 2001; Ferin et al., 1990; Lighty, Veranth, & Sarofim, 2000; Pinkerton, 2002; Varghese & Gangamma, 2006). In this study we will synthesize ship-related particles and characterize their above-mentioned specific health related properties.

Particles emitted from ship diesel engines are mainly composed of organic carbon, sulfate and ash. Nickel and vanadium are the major components of ash and are formed by burning low-grade fuel oils (Lyyränen, Jokiniemi, Kauppinen, & Joutsensaari, 1999). Recently, Murphy et al. (2009) performed simultaneous on-board and airborne measurements of particles emitted from a modern container ship. They observed low elemental carbon to organic carbon emission ratios (EC/OC$\sim$0.04) and report particles in two size ranges: 5–8 and 30–100 nm. The 5–8 nm nanoparticles dominated the total number concentration. Transmission electron microscope (TEM) data showed that these nanoparticles were composed of vanadium, nickel and sulfur. The 30–100 nm particle range also contained vanadium, sulfur and nickel components but showed a greater presence of organic carbon. In this study, we synthesized 5–8 nm ash with similar physical and chemical characteristics, as the particles reported by Murphy et al. (2009).

5–8 nm particles can be synthesized by the spray flame pyrolysis method (Pratsinis, 2006). The flame provides an environment for liquid phase particle precursor to completely evaporate and nucleate to form nanoparticles. Particles are then formed in the post-flame region where temperature cools down. We use heavy fuel oil (HFO) as the liquid phase particle precursor and apply spray flame pyrolysis with a lab-scale oxy-hydrogen flame burner to generate ash particles. A chemical equilibrium model compares and predicts nickel and vanadium compounds from combustion conditions. Health-related PM characteristics (e.g., size, hygroscopicity, morphology and composition) of the synthesized particles are compared to the data reported in published works. The unique oxy-hydrogen flame burner has two distinct qualities. When heated the burner facilitates the flow of highly viscous HFO in the capillary tube and eliminates elemental carbon formation and contamination. To our knowledge, this is the first time ship ash PM has been aptly synthesized on a laboratory scale.

2. Experimental

2.1. Setup

Particles were synthesized using an oxy-hydrogen flame burner as shown in Fig. 1. The apparatus consists of three co-axial stainless steel tubes. The inner diameters and outer diameters of each tube are 0.5 and 0.73 mm, 1.1 and 1.5 mm, 1.8 and 12.7 mm, respectively. The innermost tube is positioned 0.5 mm higher than the other two tubes to form a nozzle on the tip of the burner. The burner is an enhanced design of the Mueller, Mädler, and Pratsinis (2003) and Guo and Kennedy (2007) burners. The new burner has a turbulent oxy-hydrogen flame. The co-axial oxygen flow provides a wider range of flame heights. The oxy-hydrogen flame is also higher in temperature compared to that of the one in Mueller et al. (2003). Various solvents can be used to dissolve particle precursors in the oxy-hydrogen flame burner. For example, HFO is more easily sprayed into the new configuration compared to the Mueller et al. (2003) design. Oxygen flow and flame height are also more easily controlled than Guo and Kennedy (2007). The current burner has simple structure and better scalability. Flame conditions such as temperature, flame height, gas velocity and residence time can be varied in wider range compared to other designs. The above features provide versatility and flexibility in flame synthesis conditions. This makes the burner an ideal tool as a standard or a reference aerosol generator. An invent disclosure was filed for this burner (Jung, Zheng, & Stovall, 2009) and for more detail see our forthcoming paper.[1]

For this study, H_2 (99.5%, Praxair) was introduced through the innermost and intermediate tubes. O_2 (99.5%, Praxair) was introduced between the intermediate and outermost tubes. Flow rates of H_2 and O_2 were controlled by mass flow controllers (647C and 1179A, MKS Instruments Inc., MA). An oxy-hydrogen flame was formed at the tip of the burner. A H_2 flow rate of 5 Lpm and O_2 flow rate of 2.5 Lpm were used in this synthesis. HFO (taken directly from the ship fuel tank same as Murphy et al. (2009) used) was first fed through the innermost tube with a syringe pump (EW-74900-00, Cole Parmer) to precisely control the feed rate. At the tip of the burner, HFO was dispersed into micrometer droplets via H_2 shear flow. The liquid droplets then underwent a series of physical and chemical processes—evaporation, combustion and nucleation-to form solid particles.

[1] Zheng, Z., Vu, H., Gidwani, A., Aguilar, G., & Jung, H. (in preparation). Development and characterization of a versatile spray flame burner for particle synthesis.

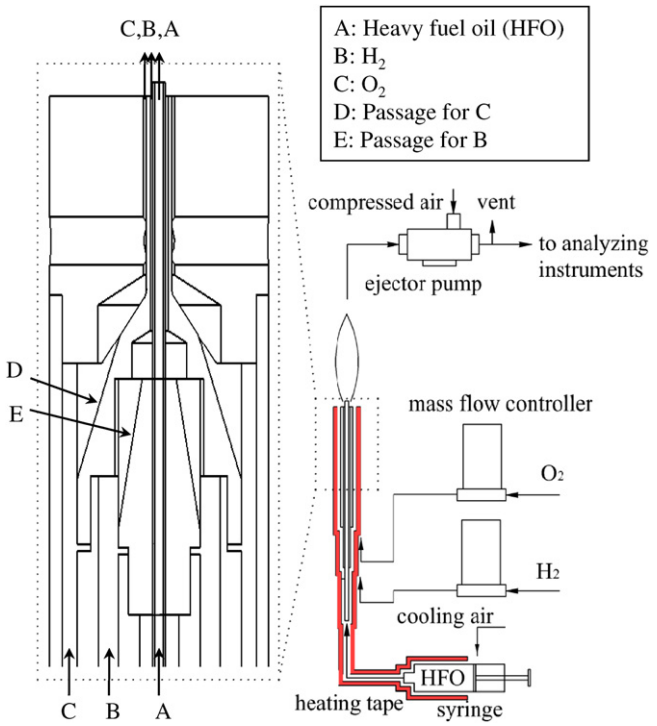

Fig. 1. Schematic of the experimental setup.

Table 1
Selected properties of HFO.

Density at 15 °C (g/ml)	0.99
Viscosity at 40 °C (mm^2/s)	743.4
Viscosity at 100 °C (mm^2/s)	31.78
Carbon (wt%)	85.87
Hydrogen (wt%)	9.63
Oxygen (wt%)	1.64
Nitrogen (wt%)	0.46
Ash (wt%)	0.072
Sulfur (wt%)	2.03
Vanadium (mg/kg)	178
Nickel (mg/kg)	58
Iron (mg/kg)	19

Chemical and physical properties of HFO are shown in Table 1. It is extremely difficult to pump and disperse highly viscous HFO at room temperature. In real-world ship engine operations, the HFO is heated up to about 100 °C to facilitate pumping and nebulization. In the current experiment, we also heated the HFO to elevated temperatures. A plastic syringe was replaced with a heat resistant stainless steel syringe (780813, KD Scientific). The syringe and oxy-hydrogen flame burner were connected by a 25 cm long stainless steel tube (outer diameter 6.4 mm). A fiberglass yarn insulated flexible heating tape (4550T131, McMaster-Carr) was wrapped around the syringe and the connecting tube to sustain temperatures higher than room temperature. A K-type thermocouple (not shown in the figure) was attached on the surface of the connecting stainless steel tube at a position close to the burner. The K-type thermocouple measured the heating temperature. The 25 cm stainless steel connecting tube provided a long enough residence time for the HFO to be heated up and reduce viscosity. A temperature controller (PM6C1CA, Watlow) controlled heating temperatures. To avoid damage, the contact surface between the stainless steel syringe and plastic syringe pump was cooled by compressed air. Particles were synthesized at HFO feeding rates of 5 and 15 ml/h and heating temperatures of 60 and 100 °C.

2.2. Sampling and characterizing

An L-shape stainless steel sampling tube (3.2 mm inner-diameter (ID), 6.4 mm outer diameter (OD) with one end facing down was placed 6 cm above the oxy-hydrogen flame tip. The other end was connected to an ejector pump (Air-Vac,

TD110H). Synthesized particles were drawn into the ejector pump and diluted. Filter samples were taken for offline chemical analysis. Particles were also analyzed with online instruments. A scanning mobility particle sizer (SMPS) measured synthesized particle size and number distribution. The SMPS was composed of a neutralizer, a differential mobility analyzer (DMA, TSI model 3080) and a condensation particle counter (CPC, TSI model 3776).

The cloud condensation nuclei (CCN) behavior of synthesized particles was characterized by a TSI 3080 SMPS (DMA 3080, CPC 3772) and a cloud condensation nuclei counter (CCNC) (Droplet Measurement Technology). Particles are size selected by the DMA and then the monodisperse aerosol stream is split. Particles of a given size are counted by the CPC and exposed to a prescribed amount of water vapor, or supersaturation, *s*, in the CCNC instrument. Particles whose critical *s* exceeds that of the instrument form droplets. The droplet number or CCN concentration is counted by an optical particle counter in the instrument (Roberts & Nenes, 2005). For this study the instrument *s* ranged from 0.18% to 0.94 $\pm$ 0.03%.

A handheld electrostatic precipitator (ESP) (Miller, Frey, King, & Sunderman 2010) was used to collect particles onto a 200 mesh copper TEM grid (3420C, SPI) for morphology characterization. A 47 mm diameter preweighed 2 μm pore size PTFE Teflon filter (Pall Gelman) was mounted on a filter holder to collect particles for PM mass and ions analysis. The volumetric flow rate passing through the filter was maintained at 20 Lpm using a critical orifice (McMaster-Carr, 3962T44) and a vacuum pump. Sampling time was 30 min. Particles were also collected on a preconditioned 47 mm diameter quartz filter (Pall, 2500 QAT-UP) for EC/OC analysis.

TEM analysis was performed at the Central Facility for Advanced Microscopy and Microanalysis (CFAMM) at UCR. TEM grid was mounted on a FEI double-tilt low background sample holder and examined at accelerating voltages of 200 and 300 kV in an FEI CM300 transmission electron microscope, equipped with an EDAX genesis energy dispersive X-ray spectrometer (EDS) fitted with Si(Li) detector. EDS analyses of the chemical composition of the particles collected on TEM grid was performed at 200 kV at tilt angle of 25° towards the detector. Loaded Teflon filter was weighed for net weight gain by a microbalance (Cahn C-35). Sulfate ions were extracted from the filter by HPLC grade water and isopropyl alcohol and analyzed using an ion chromatograph (Dionex DX-120). EC/OC content was obtained by analyzing loaded quartz filter with a Sunset Laboratory (Forest Grove) thermal/optical carbon aerosol analyzer.

3. Results and discussions

3.1. Particle size

Effects of heating temperature and HFO feeding rate on particle size distribution were investigated. Heating temperature was varied from 60 to 100 °C to simulate temperatures during ship engine operation. Two HFO feeding rates were studied, 5 and 15 ml/h. H_2 and O_2 flow rates were fixed at 2.5 and 5 Lpm in all cases.

Fig. 2 shows high heating temperature, and low feeding rate conditions lead to lower particle precursor concentration and result in smaller particle sizes. The volumetric feed rate was kept constant and as the heating temperature increased, the mass feeding rate decreased accordingly. Therefore the amount of vapors available to readily form particles was reduced.

A quenching ring (5 cm OD), as described in Teleki et al. (2009), was used to further reduce the laboratory-generated particle size to comparable ship emitted PM sizes (Jiang, 2008). The quenching device was made of a stainless steel tube

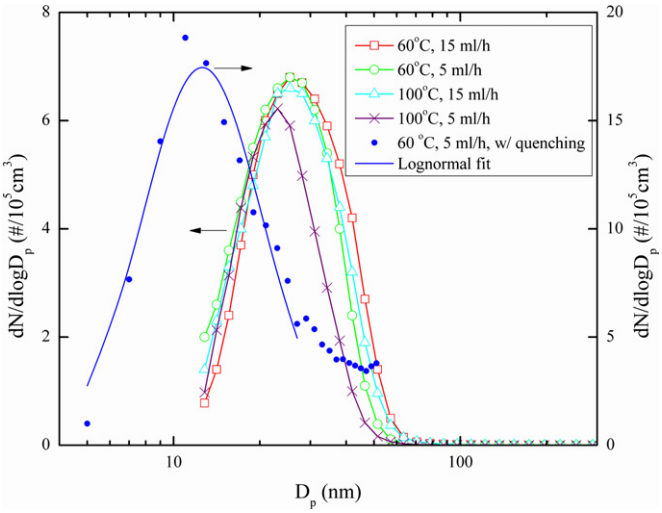

Fig. 2. Particle size distributions measured by the SMPS and the NanoDMA at different HFO flow rates and heating temperatures. The SMPS measured size distributions of particles formed without a quenching ring. The NanoDMA measured size distributions of particles formed with a quenching ring. A lognormal fit was applied to NanoDMA data.

(6.4 mm OD). 8 holes of 1 mm diameter were drilled inside the quenching ring so that the exiting gas formed a 10° angle with the radial direction of the quenching ring and a 20° angle with horizontal surface. The distance between the burner tip and quenching ring was set at 6 cm. N_2 gas at a gauge pressure of 2 bar and flow rate of 20 Lpm was supplied to the quenching ring and introduced into the flame zone with a 20° angle pointing downstream of the flame. Heating temperature was set at 60 °C and feeding rate was 5 ml/h. A NanoDMA (3085, TSI) measured particle size distributions with the quenching ring. Rapid cooling and dilution by N_2 slowed down the collision and sintering growth of particles and reduced particle diameter (Jiang, Chen, & Biswas, 2007). Fig. 2 shows that the mode particle diameter of synthesized ash was reduced to 11 nm, close to observed in-situ metal particle size range (Murphy et al., 2009).

3.2. Morphology

A TEM image of laboratory-generated particles is shown in Fig. 3a. These particles were collected at HFO feeding rate of 15 ml/h and heating temperature of 60 °C. In the TEM image, the majority of the particles are between 20 and 30 nm. The images are consistent with the size distribution measured by the SMPS (Fig. 2). A TEM image of particles sampled in the stack of a main engine on ocean going ship is also shown in Fig. 3b. TEM particles are sampled as in Murphy et al. (2009). Fig. 3a and b shows that synthesized particles have similar morphology to particles emitted from ship. The synthesized particles are slightly larger in diameter (mode of 11 versus 5–8 nm). Varying synthesis conditions and adding a quenching ring, smaller particles that better represent actual ship emitted particles may be achieved (Fig. 2). EDS analysis of synthesized particles showed sulfur and vanadium peaks similar to actual ship emitted particles (Murphy et al., 2009).

3.3. Chemical composition

Results of EC/OC and anion analysis are shown in Table 2. About 60% of total PM mass was OC and no EC was present on the filter. Ash content was obtained by subtracting EC and OC mass from the total PM mass. The absence of EC and OC to ash ratio measured in our study was very similar to those of Murphy et al. (2009) for ship PM measured on-board (Table 3). The spray flame used generated a much smaller fraction of particulate sulfate compared to real ship PM. This is likely due to the absence of a long exhaust pipe in the laboratory test. Gaseous SO_2 can convert to SO_3 and H_2SO_4 given sufficient residence times; most of the synthesized sulfur emission was in the form of SO_2.

3.4. Chemical equilibrium calculation

A chemical equilibrium calculation is a useful tool to understand the possible combustion products of metal containing fuels (Abdul-Khalek, Kittelson, Wei, & Graskow, 1998; Jang et al., 2007). The calculations were applied to a low-speed

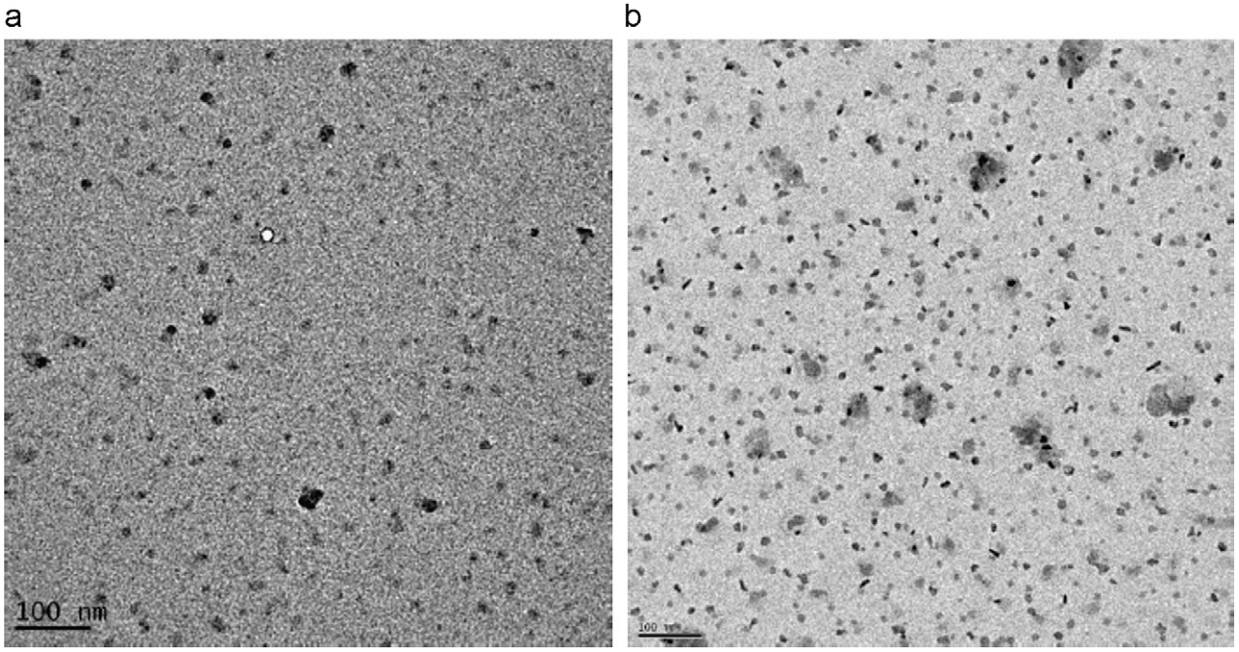

Fig. 3. TEM images of (a) synthesized particles for a feeding rate of 15 ml/h and heating temperature of 60 °C; and (b) particles collected from the exhaust stack of an ocean going vessel when the main engine was in operation.

Table 2
EC/OC and anion offline filter analysis.

PM (μg)	55.6
OC (μg)	34.1
EC (μg)	0
Ash (μg)	21.5[a]
$H_2SO_4 \cdot 6.5H_2O$ (μg)	0.00032

[a] Ash content was obtained by subtracting EC and OC mass from the total PM mass.

Table 3
Input parameters for oxy-hydrogen flame chemical equilibrium predictions.

H_2 flow rate (Lpm)	5
O_2 flow rate (Lpm)	3.5
HFO feeding rate (ml/h)	15

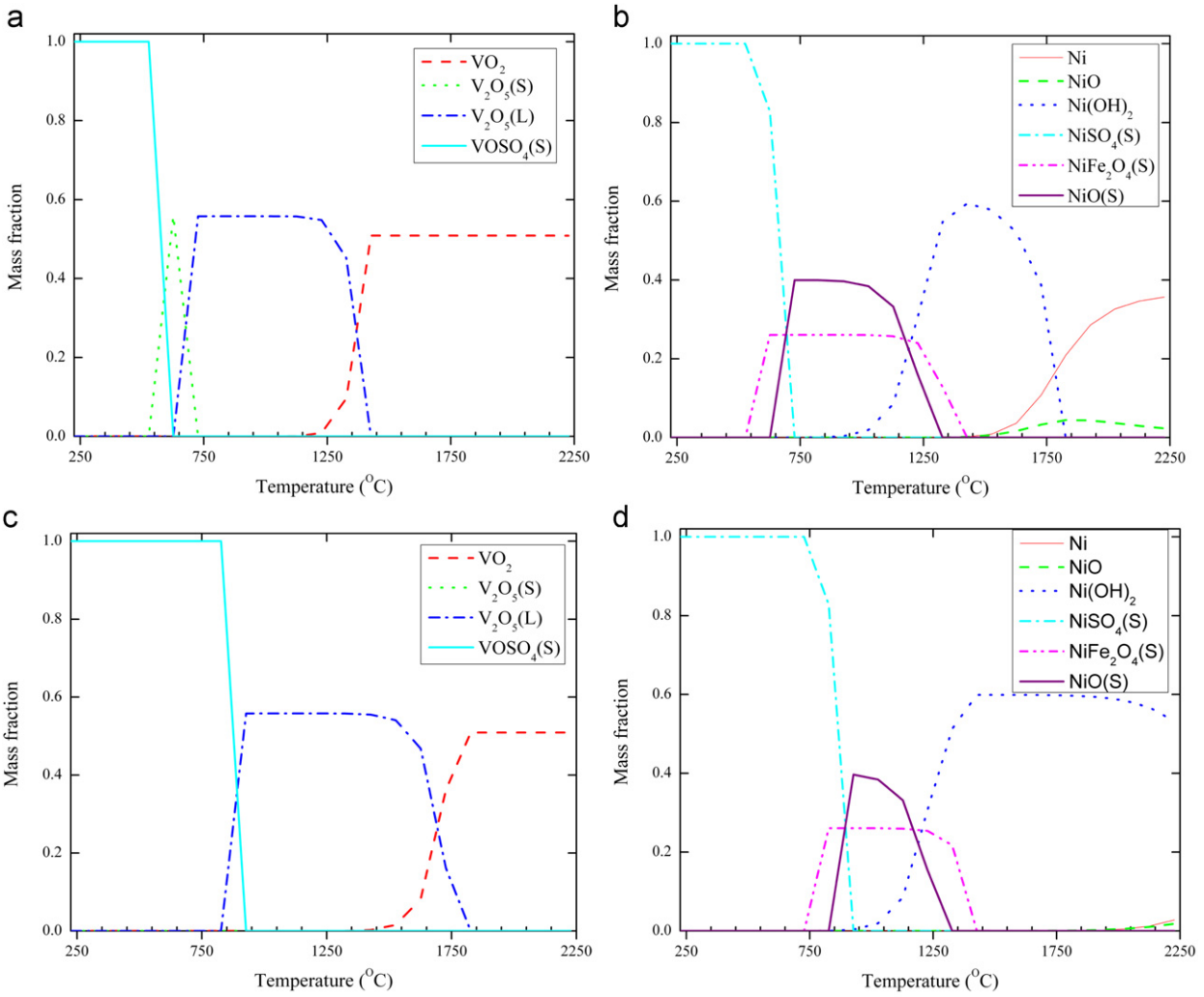

Fig. 4. Equilibrium mass fractions for ship diesel engine combustion conditions: (a) vanadium compounds at 1 bar condition, (b) nickel compounds at 1 bar condition, (c) vanadium compounds at 100 bar condition and (d) nickel compounds at 100 bar condition.

2-stroke main engine and our lab-scale oxy-hydrogen flame to predict equilibrium concentrations of vanadium and nickel containing compounds. The National Aeronautics and Space Administration (NASA) computer program Chemical Equilibrium with Applications (CEA, version 2) (Gordon & McBride, 1994) with Java graphical user interface was used. A thermodynamic input file including vanadium, nickel and sulfur properties was used (Linak, Miller, & Wendt, 2000; Linak et al., 2004). The chemical equilibrium model confirmed that the real-world ship diesel engine and synthesized flame burner combustion processes produced the same vanadium, nickel and sulfur PM products as detailed in the following sections.

3.4.1. 2-Stroke engine

For the 2-stroke main engine, 1 and 100 bar operating conditions were used. The chemical composition of HFO in Table 1 was used for predictions. The equivalence ratio of combustion was calculated as 0.6 from Man B&W Diesel Report (ManDiesel, 2004). At 1 bar, all vanadium and nickel compounds, mostly VO_2 and Ni, were in the gas phase for combustion temperatures above ~1700 °C (Fig. 4a and b). Liquid phase V_2O_5(L) was predicted at intermediate temperatures (between 600 and 1400 °C). The liquid phase was converted to solid phase V_2O_5(S) at lower temperature ranges (500–700 °C). Gas phase $Ni(OH)_2$ dominated nickel compounds between 1300 and 1700 °C. At intermediate temperatures (700–1100 °C), solid phase $NiSO_4$(S) and $NiFe_2O_4$(S) became dominant. As temperatures decreased, solid sulfate compounds were dominant. $VOSO_4$(S) and $NiSO_4$(S) were formed below 600 and 700 °C, respectively. At 100 bar, $NiSO_4$(S) and $VOSO_4$(S) solidified at higher temperatures (200–300 °C; Fig. 4c and d). The chemical equilibrium model predicted two major differences in the (1) presence of solid phase V_2O_5(S) at 1 bar between 500 and 800 °C and (2) in the dominance of gas phase $Ni(OH)_2$ at 100 bar above 1300 °C.

3.4.2. Oxy-hydrogen flame

Input parameters for the chemical equilibrium prediction of oxy-hydrogen flame are shown in Table 3. It is assumed that particles are formed in the post flame region where the equivalence ratio is low (in other words, oxygen rich) and temperature cools down (Guo & Kennedy, 2007). This assumption is supported by the observed particle size reduction from the adoption of the quenching ring in the post flame region (Fig. 2). Temperature of the current oxy-hydrogen flame was calculated for different equivalence ratios. All predicted flame temperatures were greater than 1400 °C. This result also supports assumptions of particle formation in the post-flame region. Oxygen flow rate of 3.5 Lpm was used for calculation instead of the experimental value 2.5 Lpm to simulate ship diesel engine conditions and have an equivalence ratio of 0.6 as described previously. As can be seen in Fig. 5a and b, changes in nickel and vanadium compounds for oxy-hydrogen flame have similar trends as the 1 bar case for the ocean going ship 2-stroke diesel engine. This supports that the lab-scale oxy-hydrogen burner is a useful device to generate the same type (or at least similar) particles to ship emitted particles. This study confirms the formation of vanadium and sulfur compounds during both real engine combustion and oxy-hydrogen flame combustion.

3.5. Hygroscopicity

CCN experiments characterized and compared the hygroscopicity of laboratory-generated particles to those described in Murphy et al. (2009). CCN measurements were conducted for flame conditions at 15 ml/h and 60 °C. The amount of

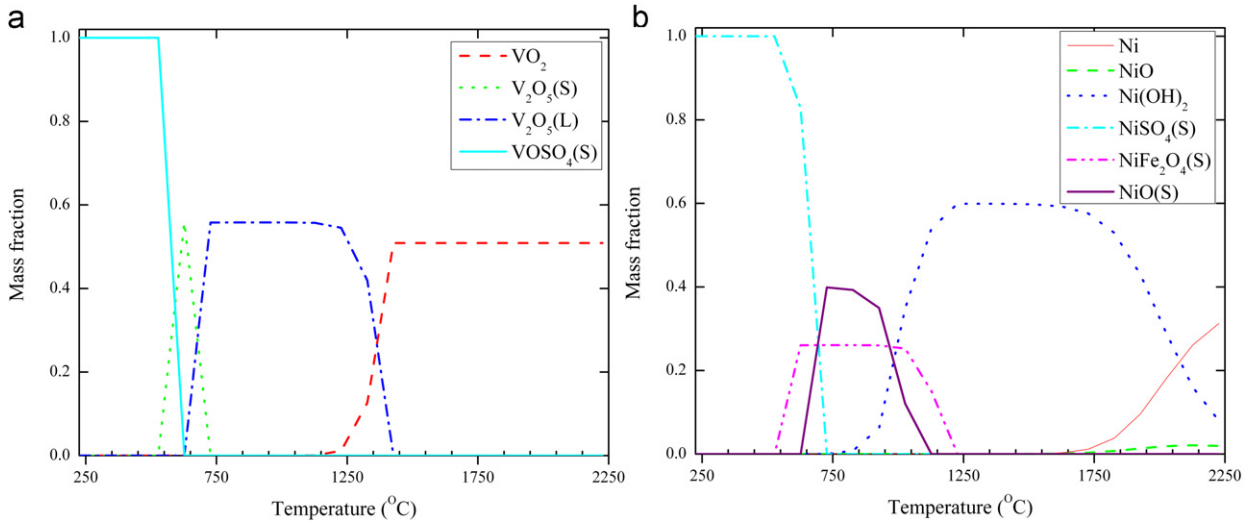

Fig. 5. Equilibrium mass fractions for synthesizing combustion conditions: (a) vanadium compounds and (b) nickel compounds.

water vapor, the supersaturation in the instrument ranged from 0.18% to 0.94%. At low supersaturations ($s < 0.8\%$) a small fraction of nuclei (< 10% of particles with size > 100 nm) formed droplets above the size of the optical particle counter detection limit (0.75 μm). This was expected, as the majority of particles from the flame study were very small insoluble metals. At $s = 0.94 \pm 0.03\%$, the particle critical diameter was ~90 nm; above this size 70% of the total particle concentration became active and formed droplets. For the same CCNC instrument conditions ($s = 0.94\%$) calibration $(NH_4)_2SO_4$ particles activated above 29 nm. The HFO particles formed by flame pyrolysis are thus much less hygroscopic than soluble inorganic species. It is noted that the condensation of gasses was minimized and the potential soluble particulate contributions from sulfates were significantly reduced in this study. However, $VOSO_4$(S), formed below 600 °C, did not enhance CCN activity. Despite the reduction in sulfate containing compounds, these CCN results are consistent with Murphy et al. (2009) who also show low CCN activity and very low hygroscopicity for real-world ship PM emissions .

4. Conclusions

Alternative particles of ash PM emitted from ships were generated in the lab using an oxy-hydrogen spray flame burner. With the aid of a quenching ring, at heating temperature of 60 °C and feeding rate of 5 ml/h, laboratory-generated particles have a peak size of 11 nm, close to that of real ship emitted ash particles. Sulfur and vanadium signals were observed in both laboratory-generated and real ship emitted particles. The absence of elemental carbon in laboratory-generated particles is comparable to the nano-mode (e.g. 5–8 nm) ship emitted particles. Chemical equilibrium calculations showed that flame synthesis condition can predict the same particle product as that of ship diesel engine. Both laboratory-generated and ship emitted particles are not hygroscopic and are not very CCN active. The consistency in PM characteristics (size, morphology, hygroscopicity, composition, etc.) of synthesized ash particles to ship diesel engine ash particles will significantly affect the feasibility of ship-related PM health studies.

Acknowledgements

We would like to thank Ms. Kathy Cocker for the filter analysis, Dr. Krassimir Bozhilov at CFAMM for his help on TEM and EDS analysis and Mr. Bill Welch and Dr. Wayne Miller for providing us HFO. We also want to thank Drs. William Linak, Jost Wendt and Sheldon Davis for sharing their thermodynamic input file for the CEA calculation.

References

Abdul-Khalek, I.S., Kittelson, D.B., Wei, Q., & Graskow, B.R. (1998). Diesel exhaust particle size: Measurement issues and trends. In: *International Congress and Exposition*, Detroit, Michigan, February 23–26, 1998.

Agrawal, H., Malloy, Q. G.J., Welch, W. A., Wayne Miller, J., & Cocker, D. R., III (2008). In-use gaseous and particulate matter emissions from a modern ocean going container vessel. *Atmospheric Environment*, *42*, 5504–5510.

Albritton, D.L., & Greenbaum, D.S. (1998). Atmospheric observations: Helping build the scientific basis for decisions related to airborne particulate matter. In: *PM Measurements Reseach Workshop*, Chapel Hill, NC.

Blanchard, J. D., & Willeke, K. (1984). Total deposition of ultrafine sodium chloride particles in human lungs. *Journal of Applied Physiology Respiratory, Environmental and Exercise Physiology*, *57*, 1850–1856.

Broday, D. M., & Georgopoulos, P. G. (2001). Growth and deposition of hygroscopic particulate matter in the human lungs. *Aerosol Science and Technology*, *34*, 144–159.

Brown, D. M., Wilson, M. R., MacNee, W., Stone, V., & Donaldson, K. (2001). Size-dependent proinflammatory effects of ultrafine polystyrene particles: A role for surface area and oxidative stress in the enhanced activity of ultrafines. *Toxicology and Applied Pharmacology*, *175*, 191–199.

Dick, C. A.J., Brown, D. M., Donaldson, K., & Stone, V. (2003). The role of free radicals in the toxic and inflammatory effects of four different ultrafine particle types. *Inhalation Toxicology*, *15*, 39–52.

Ferin, J., Oberdörster, G., Penney, D. P., Soderholm, S. C., Gelein, R., & Piper, H. C. (1990). Increased pulmonary toxicity of ultrafine particles? I. Particle clearance, translocation, morphology. *Journal of Aerosol Science*, *21*, 381–384.

Gordon, S., & McBride, B.J. (1994). *Program for Calculation of Complex Chemical Equilibrium Compositions and Applications.* I. *Analysis*. National Aeronautics and Space Administration. NASA RP-1311.

Guo, B., & Kennedy, I. M. (2007). Gas-phase flame synthesis and characterization of iron oxide nanoparticles for use in a health effects study. *Aerosol Science and Technology*, *41*, 944–951.

Gwinn, M. R., & Vallyathan, V. (2006). Nanoparticles: Health effects—pros and cons. *Environmental Health Perspectives*, 114.

Jang, H.-N., Seo, Y.-C., Lee, J.-H., Hwang, K.-W., Yoo, J.-I., Sok, C.-H., & Kim, S.-H. (2007). Formation of fine particles enriched by V and Ni from heavy oil combustion: Anthropogenic sources and drop-tube furnace experiments. *Atmospheric Environment*, *41*, 1053–1063.

Jiang, J. (2008). *Studies of Nanoparticle Synthesis and Charging in the Gas Phase: Applications in Environmental Nanotechnology and Nanotoxicology*. Washington University in Saint Louis.

Jiang, J., Chen, D.-R., & Biswas, P. (2007). Synthesis of nanoparticles in a flame aerosol reactor with independent and strict control of their size, crystal phase and morphology. *Nanotechnology*, *18*, 285603.

Jung, H., Zheng, Z., & Stovall, P. (2009). Invent disclosure: Co-axial spray burner for particle synthesis.

Kasper, A., Aufdenblatten, S., Forss, A., Mohr, M., & Burtscher, H. (2007). Particulate emissions from a low-speed marine diesel engine. *Aerosol Science and Technology*, *41*, 24–32.

Lighty, J. S., Veranth, J. M., & Sarofim, A. F. (2000). Combustion aerosols: Factors governing their size and composition and implications to human health. *Journal of the Air & Waste Management Association*, *50*, 1565–1622.

Linak, W. P., Miller, C. A., & Wendt, J. O.L. (2000). Fine particle emissions from residual fuel oil combustion: Characterization and mechanisms of formation. *Proceedings of the Combustion Institute*, *28*, 2651–2659.

Linak, W. P., Miller, C. A., Wood, J. P., Shinagawa, T., Yoo, J.-I., Santoianni, D. A., King, C. J., Wendt, J. O.L., & Seo, Y.-C. (2004). High temperature interactions between residual oil ash and dispersed kaolinite powders. *Aerosol Science and Technology*, *38*, 900–913.

Lippmann, M., & Chen, L.-C. (2009). Health effects of concentrated ambient air particulate matter (caps) and its components. *Critical Reviews in Toxicology*, *39*, 865–913.
Lyyränen, J., Jokiniemi, J., Kauppinen, E. I., & Joutsensaari, J. (1999). Aerosol characterisation in medium-speed diesel engines operating with heavy fuel oils. *Journal of Aerosol Science*, *30*, 771–784.
ManDiesel. (2004). *Emission Control Two Stroke Low-Speed Diesel Engines*. Copenhagen.
Miller, A., Frey, G., King, G., & Sunderman, C. (2010). A handheld electrostatic precipitator for sampling airborne particles and nanoparticles. *Aerosol Science and Technology*, *44*, 417–427.
Mueller, R., Mädler, L., & Pratsinis, S. E. (2003). Nanoparticle synthesis at high production rates by flame spray pyrolysis. *Chemical Engineering Science*, *58*, 1969–1976.
Murphy, S. M., Agrawal, H., Sorooshian, A., Padrol̀, L. T., Gates, H., Hersey, S., Welch, W. A., Jung, H., Miller, J. W., Cocker, D. R., Nenes, A., Jonsson, H. H., Flagan, R. C., & Seinfeld, J. H. (2009). Comprehensive simultaneous shipboard and airborne characterization of exhaust from a modern container ship at sea. *Environmental Science & Technology*, *43*, 4626–4640.
Oberdorster, G. (2000). Toxicology of ultrafine particles: In vivo studies. *Philosophical Transactions: Mathematical, Physical and Engineering Sciences 3*, 2719–2740.
Oberdorster, G., Oberdorster, E., & Oberdorster, J. (2005). Nanotoxicology: An emerging discipline evolving from studies of ultrafine particles. *Environmental Health Perspectives*, 113.
Pinkerton, K. E. (2002). *A Critical Review of the Particulate Matter Toxicology Literature for Senate Bill 25 Review of the Particulate Matter Standard*. California Environmental Protection Agency/Air Resources Board.
Pratsinis, S.E. (2006). Nanoparticulate dry (flame) synthesis and applications: Overview. In: *NSTI Nanotech 2006, NSTI Nanotechnology Conference and Trade Show*, Boston, MA, United States. May 7–11, 2006.
Roberts, G., & Nenes, A. (2005). A continuous-flow streamwise thermal-gradient CCN chamber for atmospheric measurements. *Aerosol Science and Technology*, *39*, 206–221.
Teleki, A., Buesser, B., Heine, M. C., Krumeich, F., Akhtar, M. K., & Pratsinis, S. E. (2009). Role of gas-aerosol mixing during in situ coating of flame-made titania particles. *Industrial & Engineering Chemistry Research*, *48*, 85–92.
Varghese, S. K., & Gangamma, S. (2006). Particle deposition in human respiratory tract: Effect of water-soluble fraction. *Aerosol and Air Quality Research 6*, 360–379.